Sensors & Actuators: B. Chemical 379 (2023) 133213

Contents lists available at ScienceDirect

Sensors and Actuators: B. Chemical

journal homepage: www.elsevier.com/locate/snb

In-situ admittance sensing of sweat rate and chloride level in sweat using wearable skin-interfaced microfluidic patch

Lei Wei [a,b], Zihan Lv [a], Yuxin He [a], Lin Cheng [a], Ye Qiu [c], Xuanze Huang [a], Chen Ding [a], Huaping Wu [c,*], Aiping Liu [a,*]

[a] Key Laboratory of Optical Field Manipulation of Zhejiang Province, Zhejiang Sci-Tech University, PR China
[b] School of Physics and Electronics Engineering, Fuyang Normal University, Fuyang 236037, PR China
[c] Key Laboratory of Special Purpose Equipment and Advanced Processing Technology, Ministry of Education and Zhejiang Province, College of Mechanical Engineering, Zhejiang University of Technology, Hangzhou 310023, PR China

ARTICLE INFO

Keywords:
Sweat rate
Sweat chloride level
Admittance sensing
Microfluidic patch
Laser-cutting technology

ABSTRACT

Real-time, in-situ evaluation of sweat and electrolyte loss under heat stress is critical in preventing the risks of heat-related illnesses and maintaining individual's physical performance for athletes or individuals working in extreme environments. Simultaneous monitoring of sweat rate and sweat chloride concentration via wearable device could provide an accessible route to assess the wastage of fluid and electrolytes. In this work, we report a low-cost, easy-to-manufacture epidermal microfluidic patch via entire laser-cutting scheme and transfer-printing operation. Sandwich-structured sweat rate sensor with trigger sites can induce a high pulse of electrode admittance for quantifying sweat rate when advancing sweat arrives at trigger sites, which favors the sensor inherent higher noise tolerance and independence of sensing on the change of ionic charge. Sweat chloride concentration is also quantificationally analyzed by measuring the admittance of interdigital electrode embedded in the microchannel, representing a simple, practicable, and stable alternative to colorimetric and ion-selective sensors. In-vitro and on-body experiments demonstrate the feasibility and accuracy of continuous measurement for sweat rate and sweat chloride concentration by admittance sensing method. This intrinsically robust, reliable sensing performance of the skin-interfaced microfluidic patch contributes to potential development of such device in personalized medicine.

1. Introduction

Perspiration is the main physiological mode of heat dissipation to maintain the body temperature in balance [1]. However, continuous exposure to high temperature or engagement in sustained, vigorous physical activities could cause excessive water loss of the body, which may compromise individual physical performance and increase the risk of heat-related illnesses, such as dehydration and hyperthermia [2–5]. Therefore, timely adequate fluid ingestion is essential to prevent the body fluid deficit during prolonged exercise or working in extreme environment [6]. However, excessive fluid intake can lead to hyperhydration that may degrade physical performance [7–9], even develop into life-threatening hyponatremia [10,11]. In order to maintain euhydration state during continuous perspiration process, real-time monitoring of sweat rate is essential for customizing personalized fluid replacement strategies [8,12–15]. In addition, sweat electrolyte level is influenced by sweat rate due to the sweat secretion and reabsorption mechanism [16–21]. Thus, simultaneous measurement of both sweat electrolyte and sweat rate can provide comprehensive insight into sweat composition. Because of the considerable variation in sweat electrolyte losses within and among individuals and in different exercise events [22], personalized fluid replacement strategies based on both sweat and electrolyte loss are recommended. Consider that chloride ion is the most abundant anion in sweat [23], simultaneous monitoring of sweat chloride concentration with sweat rate is therefore conducive to develop appropriate rehydration strategy for maintaining well physical condition.

Traditional sweat rate measurement is based on absorbent pads or gauzes, requiring post-collection analysis performed in conventional laboratory settings, which are impractical for real-time monitoring and ambulatory deployments [12,22,24]. Recently, colorimetric [12,25–29], volumetric [30,31], capacitive [32,33], impedance (or

* Corresponding authors.
E-mail addresses: wuhuaping@gmail.com (H. Wu), liuaiping1979@gmail.com (A. Liu).

https://doi.org/10.1016/j.snb.2022.133213
Received 15 July 2022; Received in revised form 14 December 2022; Accepted 18 December 2022
Available online 21 December 2022

admittance) [17,18,34–39], and calorimetric [40] sensing methods have been developed for in-situ measurement of sweat rate, but several challenges remain. Colorimetric and volumetric sensing methods require visual access to optical images which is inconvenient to automatic monitoring. Impedance method allows continuous and real-time monitoring, but the variable salinity of sweat can confound measurement accuracy of sweat rate, so the calibration with sodium ion concentration is usually required [17,34]. In addition, embedding two parallel microelectrodes into spiral or serpentine microchannel requires precise alignment operation [17,18,34,35]. Although the electronic based sweat rate sensor enables the monitoring of sweat rate without manual intervention, the continuous electrical signal output from sensor is susceptible to motion and ambience noise. By contrast, the use of pulse-style signal trigged by given sensing incident can effectively isolate the noise effects. For example, Francis et al. [37] and Yuan et al. [38] successively designed sweat rate sensors that could output pulse signal to characterize sweat rate. However, pre-calibration to individual sensing unit is still necessary [37], and the sensor performances of temporal resolution and noise tolerance need further improved [38]. Moreover, the sweat chloride concentration quantification using wearable device is reported based on colorimetric [12,25,29] or potentiometric [41,42] methods. Colorimetric method usually requires reference color mark for calibration of variable lighting conditions, while potentiometric sensor usually requires multistep, time-consuming manufacturing procedures.

In this work, we propose an integrated microfluidic patch with sweat rate sensor and sweat chloride concentration sensor (Fig. 1 and Fig. S1). A sandwich structure is used to construct the sweat rate sensor by arranging two electrodes on the upper and the bottom sides of microchannel layer (Fig. 1a). A trigger site array is defined at the intersections of microchannel and upper/bottom electrodes, as the black points illustrated in Fig. 1b, where sweat can simultaneously wet both electrodes (Fig. 1c). The sweat rate sensor will create a high admittance pulse when advancing sweat arrives at each trigger site at specific position in microchannel (Movie S1). This admittance pulse-based sensing method can overcome the dependence of the sweat rate measurement on the change of ionic charge, and significantly enhance the noise tolerance of the sensor. The sandwich structure is conducive to produce greater admittance jump height, facilitating higher reliability and fidelity of the collected signal. Besides, an interdigital electrode for admittance-based sensing of sweat chloride concentration is integrated into sweat collection layer (Fig. 1d). The entire patch manufactured by laser-cutting and transfer-printing technology has a diameter of about 20 mm, smaller than a 1-yuan coin (Fig. 1e) and can be conveniently integrated with a flexible printed circuit board (FPCB) to form in-situ sweat sensing system (Fig. 1f) which can easily accommodate to skin contour on different parts of the body, such as the forearm, forehead, and back (Fig. 1g), and perform reliable sweat collection (Fig. S2) and sensing signal acquisition via the FPCB.

Supplementary material related to this article can be found online at doi:10.1016/j.snb.2022.133213.

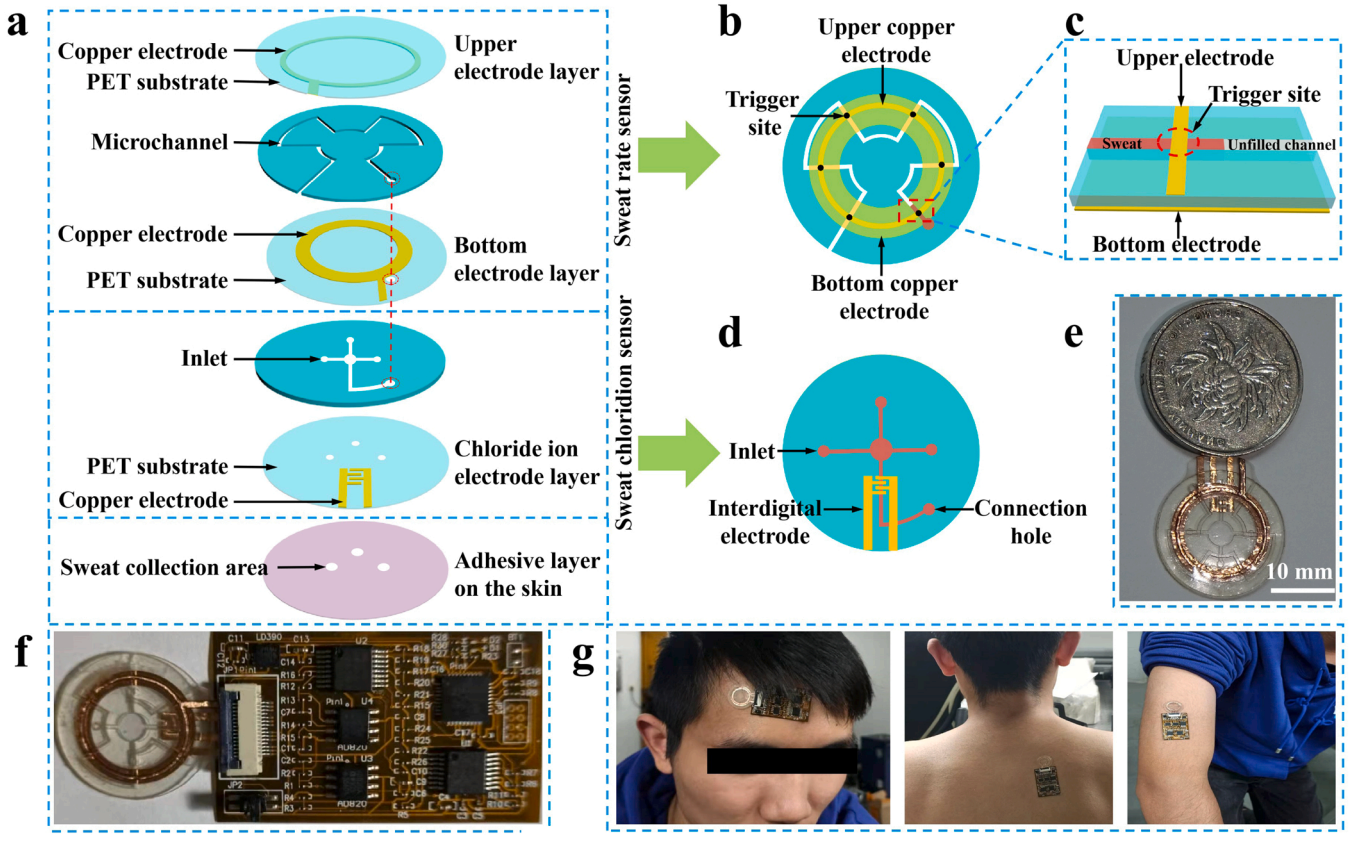

Fig. 1. Overall design of the epidermal microfluidic patch for in-situ admittance sensing of sweat rate and sweat chloride concentration. (a) Schematic drawing of the patch in an exploded view format to illustrate the different layers. (b) Top view of sweat rate sensor to elaborate the component layout and the position of trigger site. (c) Illustration of the 3D structure of trigger site where sweat can wet two electrodes simultaneously. (d) Top view of sweat chloride ion sensor and sweat collection layer consisting of three sweat collection inlets, accumulation reservoir, and a pair of interdigital electrodes. (e) Photographic image of the microfluidic patch when comparing with a 1-yuan coin to visualize the size of the patch. (f) The microfluidic patch integrated with a FPCB (g) can be conveniently mounted on the skin surface of different parts of the body.

2. Material and methods

2.1. Fabrication of the microfluidic patch

The fabrication method and process of the microfluidic patch involved laser-cutting, transfer-printing, and assembling of each layer (Fig. S3). For electrode layer manufacturing, a flexible copper foil tape (50 μm in thickness, Double conductive copper foil tape, Shenzhen baojiasheng adhesive tape products factory, China) was first adhered onto a low adhesive tape (Youbisheng Adhesive tape, Hangzhou Co. LTD, China), letting the sticky side up (Fig. S4a). Then, a laser cutter (ultraviolet laser marking machine-3 W, Shenzhen Chao-Yue laser Intelligent Equipment Co., Ltd., China) was used to fabricate the outline of electrode (Fig. S4b), followed by removing the excess copper foil and only remaining electrode on low adhesive tape (Fig. S4c). During this process, the positions of low adhesive tape and electrode were fixed. Then a PET film (12 μm in thickness) was pasted on the sticky side of the electrode (Fig. S4d), and the outline of the film was shaped by laser-cutting (Fig. S4e). At last, the electrode and PET film were peeled off together from low adhesive tape (Fig. S4f), then an electrode layer was obtained. This transfer-printing scheme of the electrode in this work did not involve thermal release tape and water-soluble tape, and therefore it was rapid and low-cost when compared to previously reported strategies [43,44].

For microchannel fabrication and encapsulation, a silicone board (Taizhou Huayang Chemical Technology Co., Ltd, China) was first pasted onto the worktops of laser cutter, then double sided tape (9495LE 300LSE, 3 M, USA) was pasted onto the fixed silicone board. Microchannel with 500 μm width was fabricated by laser cutting. Then the microchannel layer was transfer-printed from silicone board to PET film. The practicable transfer printing of electrode or microchannel layer was ascribed to the strong adhesion between PET film and transferred layers (Fig. S5 and Fig. S6).

2.2. Characterization of the microfluidic patch dy of our device

Electrode admittances of both sensors in in-vitro and on-body tests were measured via a FPCB (detailed designs in Fig. S7 and Fig. S8) after it integrated with the microfluidic patch (Fig. S9). The in-vitro test system was built as illustrated in Fig. S10 and Fig. S11. To characterize the response of sweat rate sensor under different injection rates, 40 mM NaCl solutions were injected into the sensor with the injection rate changing from 0.1 to 8 μL·min^{-1}. The sensing ability of the sensor to different chloride ion concentrations was studied by injecting NaCl solutions (10–100 mM) into the sensor with a constant rate of 0.5 μL·min^{-1}. The quadrate sandwich structured sweat rate sensing patches with different numbers of trigger site were also fabricated to explore into the sensor capability of regulating temporal resolution.

The sensing performance of sweat chloride ion sensor was characterized by the electrochemical impedance spectroscopy (EIS) via the electrochemical workstation (CHI 660E, Shanghai Chenhua Instrument Co., Ltd, China) under different copper ion concentrations (50 mM NaCl solutions containing various copper ion) and different NaCl concentrations (12.5–100 mM with 15 μM copper ion), respectively. The impacts of cations (NaCl, KCl and $CaCl_2$) and injection rates (0.5, 1.0, 2.0 μL·min^{-1}) on sensor performance were carried out by the admittance-based sensing method, respectively.

2.3. On-body test of the microfluidic patch

The on-body test of the microfluidic patch was carried out on six healthy young volunteers (Subject I to VI) at different body parts (chest, back, forearm and forehead) to study the regional variations in sweat rate and chloride concentration. Each volunteer had been given full, informed consent before participating in the test. Dyeing reagent was deposited at the inlet of the microfluidic patch to highlight the sweat entering microchannel. The microfluidic patches were attached to the volunteers' skin by double-sided tape (9495LE 300LSE, 3 M, USA). Sweat was induced by performing stationary biking and being exposed to high temperature. The admittance information was recorded and saved by FPCB during the trials. Besides, three sweat absorbent patches as control for sweat rate measurement were also pasted to the adjacent locations of the microfluidic patch to verify its sensing performance. The absorbent patch was peeled off and weighed with a precision balance when sweat arrived at the first, fourth and seventh trigger site. The real sweat volume in microchannel was acquired by recording the optical image of the dyed sweat. The sweat rate calculated from image-based sweat volume was used as the reference to assess the accuracy of microfluidic sweat sensor. After on-body measurement of sweat rate and chloride concentration, the collected sweat in microchannel was extracted by a syringe and used to measure the average sweat chloride concentration with a commercial portable chloride meter (CLS-10B, Qingdao Lintuo Environmental Technology Co., Ltd, China).

3. Results and discussion

3.1. In-vitro characterization of the microfluidic patch

3.1.1. Sensing principle and performance of the sweat rate sensor

The section view of the partial microchannel of sweat rate sensor is illustrated in Fig. 2a. Narrow upper electrode determines the position of trigger sites where sweat can simultaneously wet both electrodes. In this way, electrodes and sweat together form a current path at the trigger site. An equivalent circuit model is illustrated in Fig. 2b to show the conduction mechanism at the trigger site, where C_d and R_{ct} represent the double layer capacitance and charge-transfer resistance between the electrode-electrolyte interface, respectively. R_s and Z_w are solution resistance and Warburg diffusion impedance, respectively. The equivalent circuit at each trigger site can be reducible to an admittance. When sweat meniscus (the most anterior part of the sweat in the microchannel) arrives at a trigger site, an admittance is in parallel connected into the circuit between two electrodes (Fig. 2c), and the total admittance between two electrodes (abbreviated as electrode admittance) stepped increases meanwhile. When the sweat meniscus is between two adjacent trigger sites, the electrode admittance remains constant. Thus, electrode admittance presents a stepped curve when the sweat advances along the microchannel (Fig. 2d and Movie S1). The pulse of electrode admittance difference (abbreviated as admittance pulse) emerges once sweat meniscus arrives at a trigger site (Fig. 2e and Movie S2). The admittance pulse can serve as a stopwatch to stamp time-marking for each trigger site by recording the arriving moment of sweat meniscus. Time span between adjacent time-marking determines the mean sweat rate of this period (denoted as $Q_{i\text{-}0.5}$), which can be calculated by.

Supplementary material related to this article can be found online at doi:10.1016/j.snb.2022.133213.

The sensing performance of the microfluidic patch is tested by the self-built measurement platform (Fig. S10 and Fig. S11). NaCl solution is used as test solution due to the dominant concentration of chloride ion and sodium ions in sweat. The response of sweat rate sensor to different injection rates (from 0.1 to 8 μLmin^{-1}) and different concentrations of NaCl solution (from 10 to 100 mM) which cover entire physiological rang were investigated, respectively. The measured electrode admittance can be denoted as $\boldsymbol{Y}$= [Y_1, Y_2, …, Y_m, …]. The admittance changes under different injection rates are illustrated in Fig. 3a, Fig. S12a, Fig. S13a and Fig. S14a. The admittance difference sequence obtained by subtracting Y_i from Y_j ($i < j$) is denoted as $\boldsymbol{\Delta Y}$= [ΔY_1, ΔY_2, …, ΔY_m, …], where ΔY_m=Y_m-$Y_{m+i\text{-}j}$ and the value of (j-i) are denoted as differential step. The difference sequence contains a range of admittance pulses, as shown in Fig. 3b, Fig. S12b, Fig. S13b and Fig. S14b. It can be found that the pulse emerged more frequently at higher injection rates. The straight part in electrode admittance curve and the baseline in admittance difference curve mean that sweat meniscus is between two

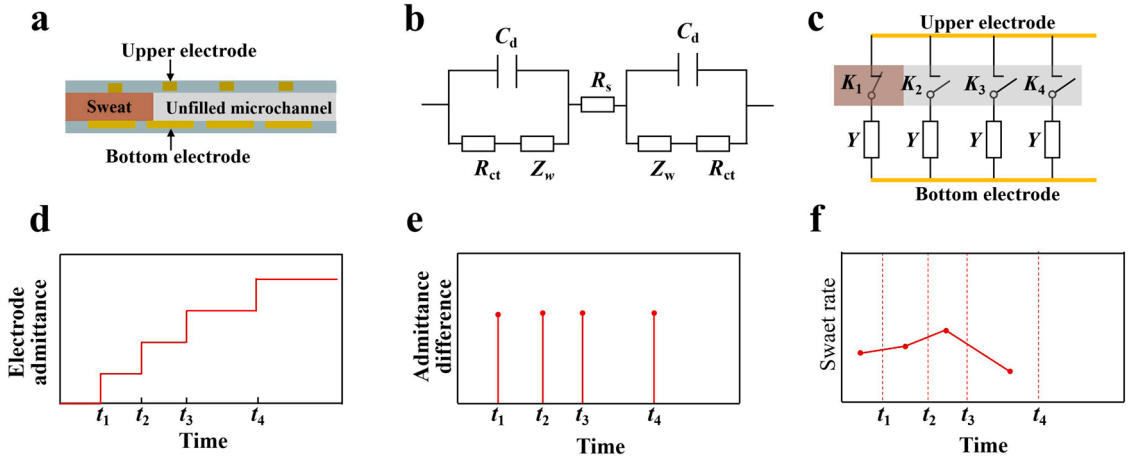

Fig. 2. Principle of sweat rate measurement based on a sandwich structured microfluidic sensor. (a) The section view of partial microchannel of the sweat rate sensor. (b) The equivalent circuit model between two electrodes at trigger site under sinusoidal excitation voltage. (c) The schematic of how admittance is successively connected into the circuit of electrode. The *Y* in this drawing represents the equivalent admittance of the circuit in Fig. 2b at each trigger site. (d) Electrode admittance signal of the sweat rate sensor. (e) Admittance difference signal derived from total admittance signal. (f) Sweat rate obtained from Fig. 2e by Eq. (1).

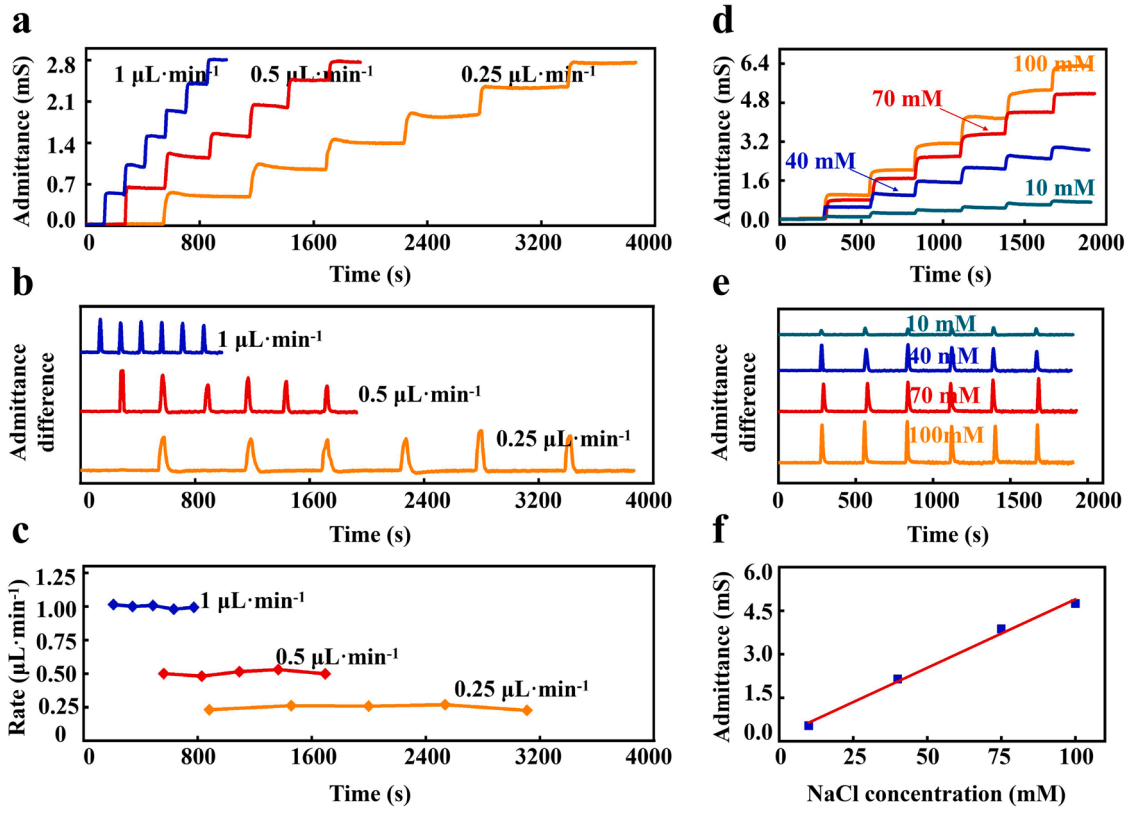

Fig. 3. Performance characterization of sweat rate sensor. (a) Electrode admittance in 40 mM NaCl solution at different injection rates, (b) corresponding admittance difference signals and (c) sweat rates derived from admittance difference information. (d) Electrode admittance of NaCl solutions with different concentrations at an injection rate of 0.5 μL·min^{-1}, and (e) corresponding admittance difference signals. (f) Calibration curve between electrode admittance and NaCl concentration in Fig. 3d illustrates linear increase in admittance magnitude with NaCl concentration.

adjacent trigger sites at that time, while the step and the pulse correspond to the moment that sweat meniscus is passing through the trigger site. So admittance pulses can be used to stamp time-markings for every trigger sites. As it always takes a while to completely wet the upper electrodes at trigger sites, the change of admittance curve at the step presents gradual increase instead of sudden jump. The corresponding pulse is peaky curve with specific width rather than a single point impulse and the width will be enlarged at lower injection rates (Fig. 3b and Fig. S12b). The measured injection rates can be obtained according to time-marking information stamped by admittance pulse. As Fig. 3c, Fig. S13c and Fig. S14c shown, this measured injection rate is consistent with the true injection rate, and the average measurement error is less than 4% at each injection rate (Fig. S15). The detection limit of the sweat rate sensor can be calculated to be 0.5 nL•min^{-1} in the case that the signal-to-noise ratio is 3 [45,46]. The step height of the electrode admittance curve is about 500 μS which is two orders of magnitude

larger than that reported in Reference [38,39], revealing the improved noise tolerance of our sensor due to the larger amplitude of output signal. In addition, the concentration of NaCl test solution only affects the pulse signal intensity of sweat rate sensor at a certain injection rate. Although both step heights of electrode admittance curve and admittance pulse increase with electrolyte concentration, their frequencies remain constant (Fig. 3d-e). This demonstrates that the proposed approach of sweat rate measurement is unaffected by sweat conductivity change, highlighting the advantage of the pulse-type sweat rate measurement when compared to previously reported continuous sweat rate sensors [17,34–36]. Fig. 3f shows that when test solution fills the microchannel, the electrode admittance is approximately proportional to electrolyte concentration, implying the dominant proportion of solution conductance in the electrode admittance. Besides, to fully demonstrate the robustness of the sweat rate sensor, we also conduct the experiment of sweat rate sensing under different pH solution, the results indicate that the sensor based on copper electrode can perform stable sensing under acid and alkaline environments of sweat level (Fig. S16) and present good reproducibility (Fig. S17). This pulse-style measurement method presents better stability because it can avoid adverse effect of output signal drift on sensing accuracy. Particularly, in the sandwich-structured sweat rate sensor, two electrodes are arranged on the upper and lower sides of the microchannel layer, in this case the conductance of the electrodes is

$$G_s = \kappa \frac{A_{ov}}{h}, \tag{2}$$

where κ is the sweat conductivity, h is the microchannel height, A_{ov} is the area of overlapping parts between the electrodes and microchannel at the trigger site. As h is very small, the height of admittance step is large, which enables high noise tolerance and strong robustness.

The sweat rate measured above is a mean value between two adjacent time-marking. We can enhance temporal resolution of sweat rate measurement by reducing the spacing of adjacent trigger sites. In order to intuitively demonstrate the scheme feasibility for flexible regulation of temporal resolution, we fabricated a square patch of sweat rate sensor, as illustrated in Fig. S18a. One of the electrodes in the sandwich structure is parallel to microchannel (called as parallel electrode), while the other electrode is perpendicular to microchannel (called as perpendicular electrode) (Fig. S18b). Arrayed trigger sites are constructed at the intersection of perpendicular electrode and microchannel (Fig. S18c). The amount of trigger site can be easily regulated by changing the numbers of cross line (from 1 to 4) in perpendicular electrode (Fig. S18d). Our results show that time interval between two pulses decreases with the increase of cross line numbers (Fig. S18f). The admittance is proportional to the amount of trigger sites (Fig. S18e and Fig. S18g), implying that the step height maintains constant when the temporal resolution increases. This means that this sweat rate sensor resolves the conflict between the resolution and noise tolerance of the sweat sensor in previously reported work [38], namely adding the number of the cross lines can increase multiple temporal resolution without the degeneration of noise tolerance. However, current response of electrode will increase with activating more trigger sites, which may lead to the overflow of AD converter. We can avoid the adverse result through choosing sinusoidal excitation signal with low amplitude or setting an in-phase amplifier circuit to reduce the amplitude of signal input to AD converter.

3.1.2. Sensing performance of admittance-based sweat chloride ion sensor

Chloride ion is the most abundant anion in sweat, so its concentration governs the sweat conductivity. We use sweat admittance to quantify chloride ion level in sweat. We first focus on the impact of chloride ion concentration and copper ion concentration on R_{ct} by EIS measurement. The EIS Nyquist plot of the copper electrode in 50 mM NaCl solution with different copper ion concentrations is displayed in Fig. S19 (the curves with different chloride ion are plotted in Fig. 4a). The semicircle part in EIS curves corresponds to R_{ct}. The smaller R_{ct} is obtained at higher copper ion concentration or at lower chloride ion concentration. The change of copper ion concentration presents a more significant impact on R_{ct} than chloride ion concentration. Considering the typical ion concentration in sweat (15 μM for copper ion and 25 mM for chloride ion), we can obtain the$R_{ct}/2 = 0.6 \times 10^5 \Omega$ according to the EIS curves in Fig. 4a, and then the double-layer capacitance C_d is given as [47].

$$C_d = \frac{1}{\omega_B R_{ct}}, \tag{3}$$

where $\omega_B = 7$ Hz corresponds to the frequency at the vertex of an EIS semicircle. The capacitive reactance X_C of C_d is

$$X_c = \frac{1}{2\pi f_c C_d}, \tag{4}$$

where f_c is the frequency of excitation voltage (100 kHz). Therefore, we can obtain $X_c = 8.4\ \Omega$. It can be found that R_{ct} is far larger than X_c, implying that the vast majority of current passes through double-layer capacitance, while the electrochemical behavior is almost negligible. When chloride ion concentration is 25 mM, the impedance of chloride ion sensing electrodes is approximate 4.7 kΩ (according to Fig. 4b), which is far larger than the magnitude of the parallel impedance of R_{ct}, C_d and Z_w (illustrated in Fig. 2b). This indicates that solution resistance (or conductance) is the dominant component in the electrode impedance (or admittance). Solution conductance is proportional to electrolyte concentration, and sweat chloride concentration can almost represent the total anion concentration. This is why copper electrode can be used for admittance-based measurement of sweat chloride concentration. More detailed discussion about the feasibility of using copper electrode for admittance-based sweat sensing is displayed in Part II of Supplementary information [48-52].

When different concentrations of NaCl solutions (from 5 mM to 125 mM) were injected into chloride ion sensing channel at the rate of 0.5 μL·min^{-1}, and the electrode admittance at each concentration was measured continuously (Fig. 4b), which is proportional to chloride ion concentration (Fig. 4c) without the effect of cation type (Fig. 4d). The detection limit of the sweat chloride sensor can be calculated to be 0.9 mM in the case that the signal-to-noise ratio is 3 [45,46]. The reproducibility of sweat chloride sensor was also studied by 10 sensors and calibrated with standard NaCl solutions. The sensors present good consistency in the response to different chloride concentrations (Fig. S20) and excellent selectivity to chloride ion (Fig. S21). Similarly, the measurement of chloride ion concentration in sweat level is scarcely influenced by copper ions of sweat level (Fig. 4e). Variable injection rate experiment indicates that the sensor is a rate-independent device (Fig. 4f), which is crucial to microfluidic based measurement of ion concentration.

3.2. On-body sweat analysis of sweat rate and sweat chloride concentration

To demonstrate on-body use of the microfluidic patch for in-situ sensing of sweat rate and sweat chloride concentration, we conducted sweat analysis trials on six volunteers' forearm (Subject I to VI) for verifying the measurement accuracy of sweat rate sensor and sweat chloride sensor. A short break was scheduled for each trial. The sweat rate measured from optical method was used as the reference. Fig. S22 illustrates the comparison of the sweat rate measured by admittance pulse-based method and image-based optical method via the microfluidic patch. Sweat rate measured by the two methods has great correlation (Fig. S23a) and small measurement error (Fig. S23b). The results display excellent agreement between the sweat rates obtained from both methods. The great accuracy of our sweat rate is attributed to

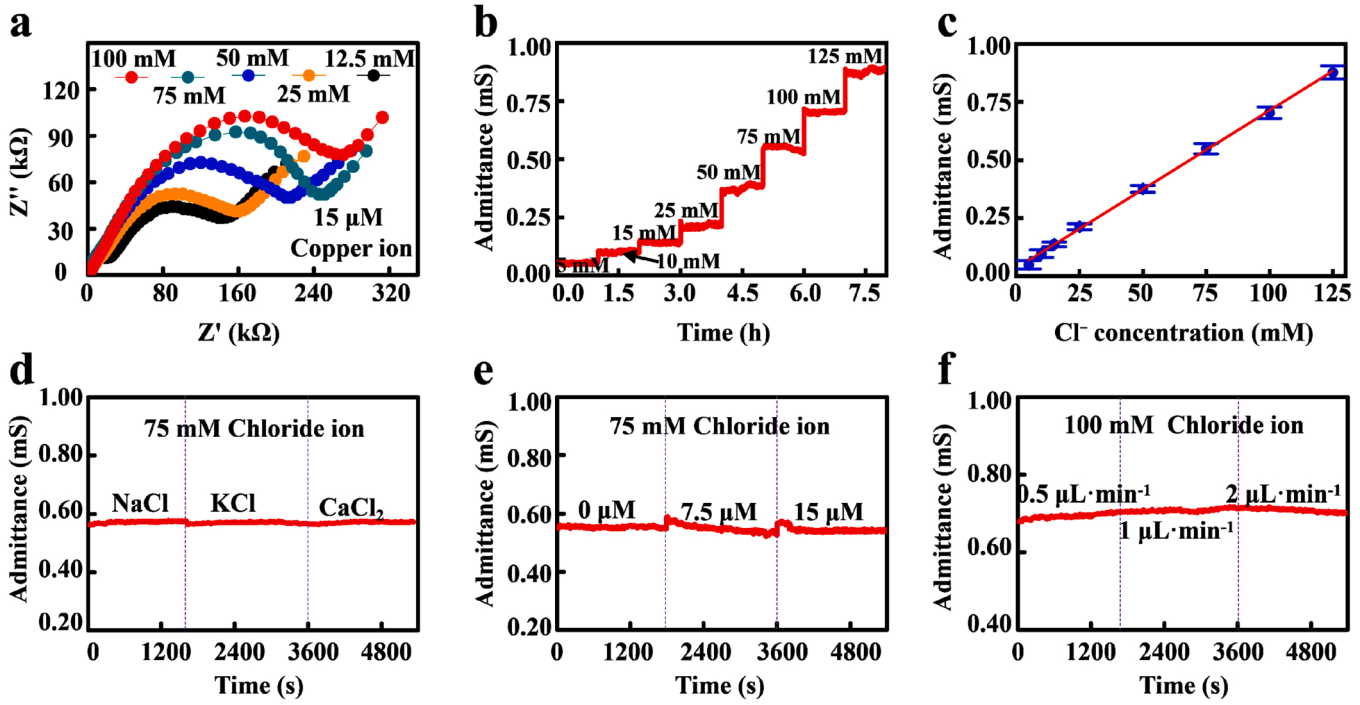

Fig. 4. Sensing performance of sweat chloride ion sensor. (a) EIS Nyquist plots of electrodes in different concentrations of chloride ion solutions with constant copper ion concentration of 15 μM. (b) Electrode admittance response to NaCl solutions with different concentrations from 5 to 125 mM. (c) Calibration curves of sweat chloride ion sensor. (d) Electrode admittance response to NaCl, KCl and $CaCl_2$ solutions with 75 mM chloride ion. (e) Electrode admittance response to 75 mM NaCl solution with different copper ion concentrations. (f) Electrode admittance response to 100 mM NaCl solutions injected with different injection rates.

pulse-type measurement method which is based on the specific incident that sweat meniscus arrives at a trigger site, rendering the sensor excellent noise tolerance and noncumulative error when compared with reported continuous sensors [17,32]. In addition, the sandwich structure allows smaller spacing between the two electrodes (450 μm in microchannel height) than that in Reference [38,39], which will provide larger admittance step and pulse amplitude (about 100–1000 $\mu S \cdot step^{-1}$, as illustrated in Fig. 3d) than those reported in Reference [38] (about 0.75–7.5 $\mu S \cdot step^{-1}$) and Reference [39] (about 0.6–6 $\mu S \cdot step^{-1}$). The larger amplitude of admittance pulse can significantly improve the noise tolerance of the sensor. More details about the advantages of our work compared with the previous studies are summarized in Table S1. Besides, sweat rate measurement based on absorbent patch (Fig. S24) and sweat chloride measurement based on commercial portable chloride

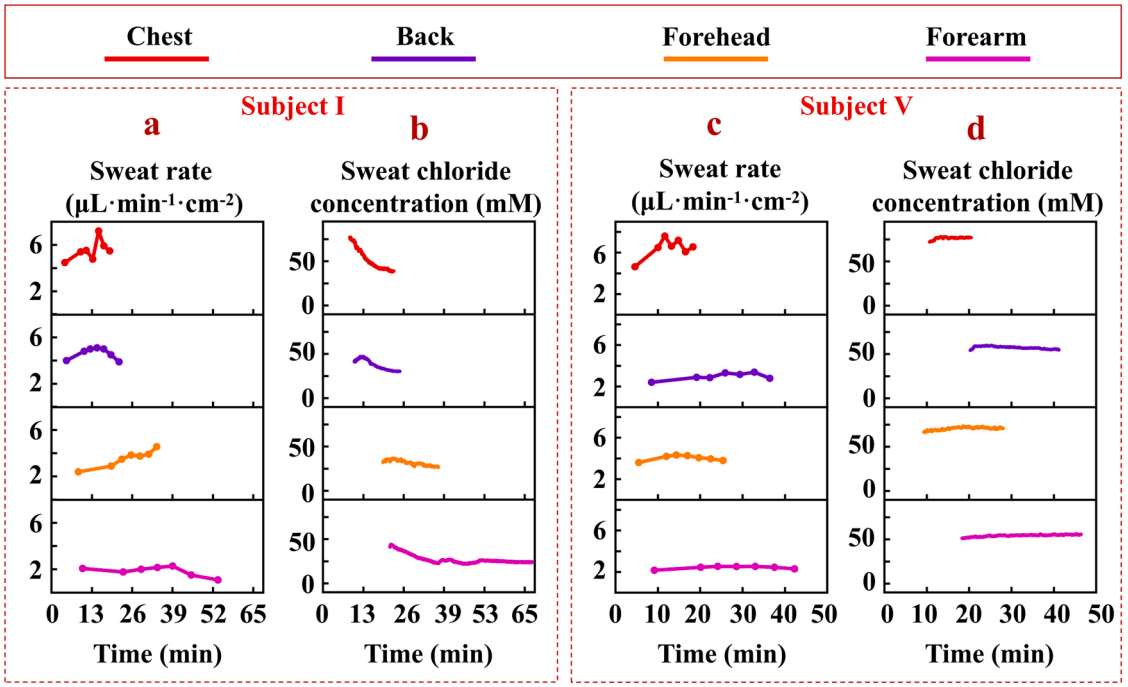

Fig. 5. Regional sweat rate and chloride concentration at chest, back, forearm, and forehead of Subject I and Subject V, respectively.

meter (Fig. S25) are further conducted, demonstrating the accuracy of the two sensors. Notice that the gravity has little effect on flow rate of the fluid in skin-interface microchannel whatever the direction of the channels in the microfluidic patch. More details are shown in Fig. S26 and Fig. S27 in Part IV in the Supporting information.

The regional variations in sweat rate and chloride concentration were also studied when the microfluidic patch was attached to the chest, back, forearm, and forehead of Subject I and Subject V, respectively (Fig. 5). For Subject I, sweat chloride concentration decreases after onset of perspiration, and eventually tend to stabilize. Especially, chloride ion at the chest shows a significant drop, approximately from 75 mM to 40 mM (Fig. 5b). By comparison, sweat chloride concentration of Subject V almost remains constant during entire trials (Fig. 5d). The difference in chloride ion concentration changes between two subjects reflects the individual variation. It can be found that sweat rate increases at the beginning of perspiration for the trials except at the forearm of Subject I (Fig. 5a and c), probably due to delayed perspiration to external stimuli. This trend is similar to the published works using other measuring approaches [17]. The forearm has the lowest sweat rate (2 $\mu L \cdot min^{-1} \cdot cm^{-2}$), while the sweat rate at chest (about 6 $\mu L \cdot min^{-1} \cdot cm^{-2}$) is higher than those at other sites in two subjects' trials. For two subjects, the chloride ion levels are more concentrated at higher sweat rates, revealing some correlations between sweat rate and sweat chloride ion level, which is consistent with previous reports [12,17,18].

4. Conclusions

In this study, we report a low-cost, easy-to-manufacture microfluidic patch capable of robustly, in-situ measuring sweat rate and sweat chloride concentration. Admittance pulse-based method provides a novel route to sweat rate measurement that is independent of electrolyte concentration. The sandwich structure in sweat rate sensor enables large admittance step height, which is a crucial parameter for high noise tolerance and excellent stability. The proposed admittance-based method for sweat chloride ion quantification represents a simple, reliable alternative to ion-selective electrode and colorimetric based methods, intrinsically preventing multistep, time-consuming sensor manufacturing procedures, and providing long-term stability and easy-to-storage features for the sweat chloride ion sensor. The high consistencies in sensing method (admittance technology), electrode material (copper foil), and manufacturing technique (laser-cutting and transfer-printing) allow for easy fabrication of the skin-interfaced microfluidic patch for detection of sweat characteristics, indicating its potential application in Human health forecast and personalized medicine.

CRediT authorship contribution statement

Lei Wei: Methodology, Software, Data curation, Writing – original draft. **Zihan Lv:** Data curation, Software, Validation. **Yuxin He:** Software, Validation. **Lin Cheng:** Formal analysis, Investigation. **Ye Qiu:** Formal analysis. **Xuanze Huang:** Formal analysis. **Chen Ding:** Formal analysis. **Huaping Wu:** Investigation, Supervision. **Aiping Liu:** Investigation, Supervision, Lei Wei ab, Zihan Lv a, Yuxin He a, Lin Cheng a, Ye Qiu c, Xuanze Huang a, Chen Ding a, Huaping Wu*c and Aiping Liu.

Declaration of Competing Interest

The authors declare that they have no known competing financial interests or personal relationships that could have appeared to influence the work reported in this paper.

Data Availability

Data will be made available on request.

Acknowledgements

This work was supported by the National Natural Science Foundation of China (Nos. 12272351, 11672269 and 11972323), the Youth Top-notch Talent Project of Zhejiang Ten Thousand Plan of China (No. ZJWR0308010), the Zhejiang Provincial Natural Science Foundation of China (Nos. LR19E020004 and LR20A020002), and the Fundamental Research Funds for the Provincial Universities of Zhejiang of China (No. RF-B2019004).

Declaration of interest statement

All the work in the manuscript is done by us independently. All authors declare that no conflict of interest exists. The manuscript is not under consideration for publication elsewhere and has not been published elsewhere in any medium including electronic journals and computer databases of a public nature.

Appendix A. Supporting information

Supplementary data associated with this article can be found in the online version at doi:10.1016/j.snb.2022.133213.

References

[1] Y. Peng, X. Cui, Y. Liu, Y. Li, J. Liu, B. Cheng, Systematic review focusing on the excretion and protection roles of sweat in the skin, Dermatology 228 (2014) 115–120, https://doi.org/10.1159/000357524.
[2] J.A. Kraft, J.M. Green, P.A. Bishop, M.T. Richardson, Y.H. Neggers, J.D. Leeper, The influence of hydration on anaerobic performance: a review, Res. Q Exerc. Sport 83 (2012) 282–292, https://doi.org/10.1080/02701367.2012.10599859.
[3] S.J. Montain, E.F. Coyle, Influence of graded dehydration on hyperthermia and cardiovascular drift during exercise, J. Appl. Physiol. 73 (1992) 1340–1350, https://doi.org/10.1152/jappl.1992.73.4.1340.
[4] S.N. Cheuvront, R.W. Kenefick, Dehydration: physiology, assessment, and performance effects, Compr. Physiol. 4 (2014) 257–285, https://doi.org/10.1002/cphy.c130017.
[5] R.P. Nuccio, K.A. Barnes, J.M. Carter, L.B. Baker, Fluid balance in team sport athletes and the effect of hypohydration on cognitive, technical, and physical performance, Sports Med 47 (2017) 1951–1982, https://doi.org/10.1007/s40279-017-0738-7.
[6] S.J. Montain, W.A. Latzka, M.N. Sawka, Control of thermoregulatory sweating is altered by hydration level and exercise intensity, J. Appl. Physiol. 79 (1995) 1434–1439, https://doi.org/10.1152/jappl.1995.79.5.1434.
[7] S.M. Shirreffs, S.J. Merson, S.M. Fraser, D.T. Archer, The effects of fluid restriction on hydration status and subjective feelings in man, Br. J. Nutr. 91 (2004) 951–958, https://doi.org/10.1079/BJN20041149.
[8] B.P. McDermott, S.A. Anderson, L.E. Armstrong, D.J. Casa, S.N. Cheuvront, L. Cooper, W.L. Kenney, F.G. O'Connor, W.O. Roberts, National athletic trainers' association position statement: fluid replacement for the physically active, J. Athl. Train. 52 (2017) 877–895, https://doi.org/10.4085/1062-6050-52.9.02.
[9] S.J. Montain, S.N. Cheuvront, M.N. Sawka, Exercise associated hyponatraemia: quantitative analysis to understand the aetiology, Br. J. Sports Med 40 (2006) 98–105, https://doi.org/10.1016/s0162-0908(08)70457-4.
[10] P.Y. Gigou, T. Dion, A. Asselin, F. Berrigan, E.D. Goulet, Pre-exercise hyperhydration-induced body weight gain does not alter prolonged treadmill running time-trial performance in warm ambient conditions, Nutrients 4 (2012) 949–966, https://doi.org/10.3390/nu4080949.
[11] E.D. Goulet, M. Aubertin-Leheudre, G.E. Plante, I.J. Dionne, A meta analysis of the effects of glycerol-induced hyperhydration on fluid retention and endurance performance, Int. J. Sport Nutr. Exerc. Metab. 17 (2007) 391–410, https://doi.org/10.1016/j.humov.2007.04.002.
[12] L.B. Baker, J.B. Model, K.A. Barnes, M.L. Anderson, S.P. Lee, K.A. Lee, S.D. Brown, A.J. Reimel, T.J. Roberts, R.P. Nuccio, J.L. Bonsignore, C.T. Ungaro, J.M. Carter, W. Li, M.S. Seib, J.T. Reeder, A.J. Aranyosi, J.A. Rogers, R. Ghaffari, Skin-interfaced microfluidic system with personalized sweating rate and sweat chloride analytics for sports science applications, eabe3929, Sci. Adv. 6 (2020), https://doi.org/10.1126/sciadv.abe3929.
[13] M.N. Sawka, L.M. Burke, E.R. Eichner, R.J. Maughan, S.J. Montain, N. S. Stachenfeld, American college of sports medicine position stand. exercise and fluid replacement, Med. Sci. Sports Exerc. 39 (2007) 377–390, https://doi.org/10.1249/mss.0b013e31802ca597.
[14] R.J. Maughan, P. Watson, S.M. Shirreffs, Implications of active lifestyles and environmental factors for water needs and consequences of failure to meet those needs, Nutr. Rev. 73 (2015) 130–140, https://doi.org/10.1093/nutrit/nuv051.
[15] S.N. Cheuvront, R.W. Kenefick, Personalized fluid and fuel intake for performance optimization in the heat, J. Sci. Med. Sport 24 (2021) 735–738, https://doi.org/10.1016/j.jsams.2021.01.004.

[16] Z. Sonner, E. Wilder, J. Heikenfeld, G. Kasting, F. Beyette, D. Swaile, F. Sherman, J. Joyce, J. Hagen, N. Kelley-Loughnane, R. Naik, The microfluidics of the eccrine sweat gland, including biomarker partitioning, transport, and biosensing implications, Biomicrofluidics 9 (2015), 031301, https://doi.org/10.1063/1.4921039.
[17] H.Y.Y. Nyein, L.C. Tai, Q.P. Ngo, M. Chao, G.B. Zhang, W. Gao, M. Bariya, J. Bullock, H. Kim, H.M. Fahad, A. Javey, A wearable microfluidic sensing patch for dynamic sweat secretion analysis, ACS Sens. 3 (2018) 944–952, https://doi.org/10.1021/acssensors.7b00961.
[18] S.B. Kim, K. Lee, M.S. Raj, B. Lee, J.T. Reeder, J. Koo, A. Hourlier-Fargette, A. J. Bandodkar, S.M. Won, Y. Sekine, J. Choi, Y. Zhang, J. Yoon, B.H. Kim, Y. Yun, S. Lee, J. Shin, J. Kim, R. Ghaffari, J.A. Rogers, Soft, skin-interfaced microfluidic systems with wireless, battery-free electronics for digital, real-time tracking of sweat loss and electrolyte composition, Small 14 (2018), 1802876, https://doi.org/10.1002/smll.201802876.
[19] L. Wei, G. Fang, Z. Kuang, L. Cheng, H. Wu, D. Guo, A. Liu, 3D-printed low-cost fabrication and facile integration of flexible epidermal microfluidics platform, Sens. Actuators B Chem. 353 (2022), 131085, https://doi.org/10.1016/j.snb.2021.131085.
[20] H.M. Emrich, E. Stoll, B. Friolet, J.P. Colombo, R. Richterich, E. Rossi, Sweat composition in relation to rate of sweating in patients with cystic fibrosis of the pancreas, Pediatr. Res. 2 (1968) 464–478, https://doi.org/10.1203/00006450-196811000-00004.
[21] A. Hoshi, H. Watanabe, M. Kobayashi, M. Chiba, Y. Inaba, N. Kimura, T. Ito, Concentrations of trace elements in sweat during sauna bathing, Tohoku J. Exp. Med. 195 (2001) 163–169, https://doi.org/10.1620/tjem.195.163.
[22] L.B. Baker, Sweating rate and sweat sodium concentration in athletes: a review of methodology and intra/interindividual variability, Sports Med 47 (2017) S111–S128, https://doi.org/10.1007/s40279-017-0691-5.
[23] A. Ganguly, S. Prasad, Passively addressable ultra-low volume sweat chloride sensor, Sensors 19 (2019) 4590, https://doi.org/10.3390/s19204590.
[24] Y. Qiu, C.J. Wang, X.Y. Lu, H.P. Wu, X.L. Ma, J.H. Hu, H.C. Qi, Y. Tian, Z. Zhang, G. J. Bao, H. Chai, J.Z. Song, A.P. Liu, A biomimetic Drosera capensis with adaptive decision-predation behavior based on multifunctional sensing and fast actuating capability, Adv. Funct. Mater. 32 (2021), 2110296, https://doi.org/10.1002/adfm.202110296.
[25] J. Choi, S. Chen, Y. Deng, Y. Xue, J.T. Reeder, D. Franklin, Y.S. Oh, J.B. Model, A. J. Aranyosi, S.P. Lee, R. Ghaffari, Y. Huang, J.A. Rogers, Skin-interfaced microfluidic systems that combine hard and soft materials for demanding applications in sweat capture and analysis, Adv. Healthc. Mater. 10 (2020), 2000722, https://doi.org/10.1002/adhm.202000722.
[26] J.T. Reeder, J. Choi, Y. Xue, P. Gutruf, J. Hanson, M. Liu, T. Ray, A.J. Bandodkar, R. Avila, W. Xia, S. Krishnan, S. Xu, K. Barnes, M. Pahnke, R. Ghaffari, Y. Huang, J. A. Rogers, Waterproof, electronics-enabled, epidermal microfluidic devices for sweat collection, biomarker analysis, and thermography in aquatic settings, Sci. Adv. 5 (2019) eaau6356, https://doi.org/10.1126/sciadv.aau6356.
[27] J. Choi, A.J. Bandodkar, J.T. Reeder, T.R. Ray, A. Turnquist, S.B. Kim, N. Nyberg, A. Hourlier-Fargette, J.B. Model, A.J. Aranyosi, S. Xu, R. Ghaffari, J.A. Rogers, Soft, skin-integrated multifunctional microfluidic systems for accurate colorimetric analysis of sweat biomarkers and temperature, ACS Sens 4 (2019) 379–388, https://doi.org/10.1021/acssensors.8b01218.
[28] A.J. Bandodkar, P. Gutruf, J. Choi, K. Lee, Y. Sekine, J.T. Reeder, W.J. Jeang, A. J. Aranyosi, S.P. Lee, J.B. Model, R. Ghaffari, C.-J. Su, J.P. Leshock, T. Ray, A. Verrillo, K. Thomas, V. Krishnamurthi, S. Han, J. Kim, S. Krishnan, T. Hang, J. A. Rogers, Battery-free, skin-interfaced microfluidic/electronic systems for simultaneous electrochemical, colorimetric, and volumetric analysis of sweat, Sci. Adv. 5 (2019) eaav3294, https://doi.org/10.1126/sciadv.aav3294.
[29] A. Koh, D. Kang, Y. Xue, S. Lee, R.M. Pielak, J. Kim, T. Hwang, S. Min, A. Banks, P. Bastien, M.C. Manco, L. Wang, K.R. Ammann, K.-I. Jang, P. Won, S. Han, R. Ghaffari, U. Paik, M.J. Slepian, G. Balooch, Y. Huang, J.A. Rogers, A soft, wearable microfluidic device for the capture, storage, and colorimetric sensing of sweat, Sci. Transl. Med. 8 (2016) 366ra165, https://doi.org/10.1126/scitranslmed.aaf2593.
[30] F.J. Zhao, M. Bonmarin, Z.C. Chen, M. Larson, D. Fay, D. Runnoe, J. Heikenfeld, Ultra-simple wearable local sweat volume monitoring patch based on swellable hydrogels, Lab Chip 20 (2020) 168–174, https://doi.org/10.1039/c9lc00911f.
[31] L. Wang, T. Xu, C. Fan, X. Zhang, Wearable strain sensor for real-time sweat volume monitoring, iScience 24 (2021), 102028, https://doi.org/10.1016/j.isci.2020.102028.
[32] D.-H. Choi, M. Gonzales, G.B. Kitchen, D.-T. Phan, P.C. Searson, A capacitive sweat rate sensor for continuous and real-time monitoring of sweat loss, ACS Sens 5 (2020) 3821–3826, https://doi.org/10.1021/acssensors.0c01219.
[33] A. Hourlier-Fargette, S. Schon, Y. Xue, R. Avila, W. Li, Y. Gao, C. Liu, S.B. Kim, M. S. Raj, K.B. Fields, B.V. Parsons, K. Lee, J.Y. Lee, H. Chung, S.P. Lee, M. Johnson, A. J. Bandodkar, P. Gutruf, J.B. Model, A.J. Aranyosi, J. Choi, T.R. Ray, R. Ghaffari, Y. Huang, J.A. Rogers, Skin-interfaced soft microfluidic systems with modular and reusable electronics for in-situ capacitive sensing of sweat loss, rate and conductivity, Lab Chip 20 (2020) 4391–4403, https://doi.org/10.1039/d0lc00705f.
[34] H.Y.Y. Nyein, M. Bariya, L. Kivimäki, S. Uusitalo, T.S. Liaw, E. Jansson, C.H. Ahn, J.A. Hangasky, J. Zhao, Y. Lin, T. Happonen, M. Chao, C. Liedert, Y. Zhao, L.-C. Tai, J. Hiltunen, A. Javey, Regional and correlative sweat analysis using high-throughput microfluidic sensing patches toward decoding sweat, Sci. Adv. 5 (2019) eaaw9906, https://doi.org/10.1126/sciadv.aaw9906.
[35] S. Kim, B. Lee, J.T. Reeder, S.H. Seo, S.-U. Lee, A. Hourlier-Fargette, J. Shin, Y. Sekine, H. Jeong, Y.S. Oh, A.J. Aranyosi, S.P. Lee, J.B. Model, G. Lee, M.-H. Seo, S.S. Kwak, S. Jo, G. Park, S. Han, I. Park, H.-I. Jung, R. Ghaffari, J. Koo, P.V. Braun, J.A. Rogers, Soft, skin-interfaced microfluidic systems with integrated immunoassays, fluorometric sensors, and impedance measurement capabilities, Proc. Natl. Acad. Sci. U. S. A 117 (2020) 27906–27915, https://doi.org/10.1073/pnas.2012700117.
[36] Y. Temiz, E. Delamarche, Sub-nanoliter, real-time flow monitoring in microfluidic chips using a portable device and smartphone, Sci. Rep. 8 (2018) 10603, https://doi.org/10.1038/s41598-018-28983-w.
[37] J. Francis, I. Stamper, J. Heikenfeld, E.F. Gomez, Digital nanoliter to milliliter flow rate sensor with in vivo demonstration for continuous sweat rate measurement, Lab Chip 19 (2019) 178–185, https://doi.org/10.1039/c8lc00968f.
[38] Z. Yuan, L. Hou, M. Bariya, H.Y.Y. Nyein, L.-C. Tai, W. Ji, L. Li, A. Javey, A multimodal sweat sensing patch for cross-verification of sweat rate, total ionic charge, and Na^+ concentration, Lab Chip 19 (2019) 3179–3189, https://doi.org/10.1039/c9lc00598f.
[39] H.Y.Y. Nyein, M. Bariya, B. Tran, C.H. Ahn, B.J. Brown, W. Ji, N. Davis, A. Javey, A wearable patch for continuous analysis of thermoregulatory sweat at rest, Nat. Commun. 12 (2021) 1823, https://doi.org/10.1038/s41467-021-22109-z.
[40] K. Kwon, J.U. Kim, Y. Deng, S.R. Krishnan, J. Choi, H. Jang, K. Lee, C.-J. Su, I. Yoo, Y. Wu, L. Lipschultz, J.-H. Kim, T.S. Chung, D. Wu, Y. Park, T. Kim, R. Ghaffari, S. Lee, Y. Huang, J.A. Rogers, An on-skin platform for wireless monitoring of flow rate, cumulative loss and temperature of sweat in real time, Nat. Electron 4 (2021) 302–312, https://doi.org/10.1038/s41928-021-00556-2.
[41] G. Xu, C. Cheng, W. Yuan, Z. Liu, L. Zhu, X. Li, Y. Lu, Z. Chen, J. Liu, Z. Cui, J. Liu, H. Men, Q. Liu, Smartphone-based battery-free and flexible electrochemical patch for calcium and chloride ions detections in biofluids, Sens. Actuators B Chem. 297 (2019), 126743, https://doi.org/10.1016/j.snb.2019.126743.
[42] L. Fan, T. Xu, J. Feng, X. Shi, C. Tian, Y. Qin, Tripodal squaramide derivative as a neutral chloride ionophore for whole blood and sweat chloride measurement, Electroanalysis 32 (2019) 805–811, https://doi.org/10.1002/elan.201900693.
[43] S. Yang, Y.C. Chen, L. Nicolini, P. Pasupathy, N. Lu, "Cut-and-paste" manufacture of multi-parametric epidermal sensor systems, Adv. Mater. 27 (2015) 6423–6430, https://doi.org/10.1002/adma.201502386.
[44] H. Jeong, L. Wang, T. Ha, R. Mitbander, X. Yang, Z. Dai, S. Qiao, L. Shen, N. Sun, N. Lu, Modular and reconfigurable wireless e-tattoos for personalized sensing, Adv. Mater. Technol. 4 (2019), 1900117, https://doi.org/10.1002/admt.201900117.
[45] S.Y. Oh, S.Y. Hong, Y.R. Jeong, J. Yun, H. Park, S.W. Jin, G. Lee, J.H. Oh, H. Lee, S.-S. Lee, J.S. Ha, Skin-attachable, stretchable electrochemical sweat sensor for glucose and pH detection, ACS Appl. Mater. Interfaces 10 (2018) 13729–13740, https://doi.org/10.1021/acsami.8b03342.
[46] S. Mani, V. Vediyappan, S.-M. Chen, R. Madhu, V. Pitchaimani, J.-Y. Chang, S.-B. Liu, Hydrothermal synthesis of NiWO4 crystals for high performance nonenzymatic glucose biosensors, Sci. Rep. 6 (2016) 24128, https://doi.org/10.1038/srep24128.
[47] E.P. Randviir, C.E. Banks, Electrochemical impedance spectroscopy: an overview of bioanalytical applications, Anal. Methods 5 (2013) 1098–1115, https://doi.org/10.1039/c3ay26476a.
[48] L.B. Baker, A.S. Wolfe, Physiological mechanisms determining eccrine sweat composition, Eur. J. Appl. Physiol. 120 (2020) 719–752, https://doi.org/10.1007/s00421-020-04323-7.
[49] N. Bagheri, V. Mazzaracchio, S. Cinti, N. Colozza, C.D. Natale, P.A. Netti, M. Saraji, S. Roggero, D. Moscone, F. Arduini, Electroanalytical sensor based on gold-nanoparticle-decorated paper for sensitive detection of copper ions in sweat and serum, Anal. Chem. 93 (2021) 5225–5233, https://doi.org/10.1021/acs.analchem.0c05469.
[50] W. Gao, H.Y.Y. Nyein, Z. Shahpar, H.M. Fahad, K. Chen, S. Emaminejad, Y. Gao, L. C. Tai, H. Ota, E. Wu, J. Bullock, Y. Zeng, D.H. Lien, A. Javey, Wearable microsensor array for multiplexed heavy metal monitoring of body fluids, ACS Sens 1 (2016) 866–874, https://doi.org/10.1021/acssensors.6b00287.
[51] P. Escobedo, C.E. Ramos-Lorente, A. Martínez-Olmos, M.A. Carvajal, M. Ortega-Muñoz, I. de Orbe-Payá, F. Hernández-Mateo, F. Santoyo-González, L.F. Capitán-Vallvey, A.J. Palma, M.M. Erenas, Wireless wearable wristband for continuous sweat pH monitoring, Sens. Actuators B Chem. 327 (2021), 128948, https://doi.org/10.1016/j.snb.2020.128948.
[52] M. Bariya, H.Y.Y. Nyein, A. Javey, Wearable sweat sensors, Nat. Electron. 1 (2018) 160–171, https://doi.org/10.1038/s41928-018-0043-y.

Lei Wei received his Bachelor Degree in Mechanical and Electronic Engineering from Inner Mongolia University of Technology in 2011, and received his master's degree in Mechanical and Electronic Engineering from Chongqing University in 2014. He is currently pursuing a Ph.D. degree in the Faculty of Mechanical Engineering & Automation at Zhejiang Sci-Tech University. His research interests include flexible electronics, microfluidic devices and wearable sweat sensors.

ZiHan Lv received his Bachelor Degree in electronic information engineering from Anhui Normal University in 2020. He is currently pursuing a master's degree in the Faculty of Mechanical Engineering & Automation at Zhejiang Sci-Tech University. His research interests are flexible electronics and its application in sweat sensing.

Yuxin He received her Bachelor Degree in the Faculty of Physics from Jilin Normal University in 2020. She is currently pursuing a master's degree in the Faculty of Science at Zhejiang Sci-Tech University. Her research interests include flexible electronics and microfluidic devices.

Lin Cheng received her Bachelor of Henan University in 2017. She is currently pursuing a Ph.D. degree in the Zhejiang Sci-Tech University. Her research interests include flexible sensor and smart materials/structures.

Ye Qiu received her Bachelor of Taizhou University in 2015. She is currently pursuing a Ph.D. degree in the College of Mechanical Engineering at Zhejiang University of Technology. She worked as a visiting scholar in Department of Mechanical Engineering at University of Colorado Boulder from 2018 to 2019. Her research interests include flexible electronics and smart materials/structures.

Xuanze Huang is currently pursuing an undergraduate degree in the department of physics at Zhejiang Sci-Tech University. Her research interests include flexible electronics and microfluidic devices.

Chen Ding is currently pursuing an undergraduate degree in the department of physics at Zhejiang Sci-Tech University. Her research interests include flexible electronics and microfluidic devices.

Prof. Huaping Wu received his Ph. D degree in Engineering Mechanics from the Harbin Institute of Technology in 2009 and a Bachelor's degree from the Harbin Institute of Technology in 2002. He worked as a visiting scholar at the Kyoto University in 2014 and a postdoctoral research fellow at the City University of Hong Kong in 2012. He is currently a Professor in the School of Mechanical Engineering at Zhejiang University of Technology. His research mainly focuses on the mechanics of smart materials/structures, bionic machinery and bionic manufacturing, and flexible electronics devices.

Prof. Aiping Liu received her Ph.D degree in Material Science from the Harbin Institute of Technology in 2008. She worked as a postdoctoral research fellow at the Nanyang Technological University from 2009 to 2011 and a visiting scholar at the University of Texas at Austin from 2019 to 2020. She is currently a Professor in the Department of Physics at Zhejiang Sci-Tech University. Her research mainly focuses on the functional inorganic/organic material, with special emphasis on developing novel materials including graphene with sensing and actuation characteristic for wearable physical/chemical sensors and intelligent actuators.